Journal of Quantitative Spectroscopy & Radiative Transfer 110 (2009) 1132–1146

Contents lists available at ScienceDirect

Journal of Quantitative Spectroscopy & Radiative Transfer

journal homepage: www.elsevier.com/locate/jqsrt

# A comparison of numerical and analytical radiative-transfer solutions for plane albedo of natural waters ☆

Leonid G. Sokoletsky [a,*], Olga V. Nikolaeva [b], Vladimir P. Budak [c], Leonid P. Bass [b], Ross S. Lunetta [d], Victor S. Kuznetsov [e], Alexander A. Kokhanovsky [f]

[a] National Research Council, National Exposure Research Laboratory, US Environmental Protection Agency, 109 T.W. Alexander Dr., Research Triangle Park, NC 27711, USA
[b] Keldysh Institute of Applied Mathematics, Russian Academy of Sciences, 4 Miusskaya Square, Moscow, 125047, Russia
[c] Moscow Power-Engineering Institute (Technical University), 14 Krasnokazarmennaya, Moscow, 111250, Russia
[d] National Exposure Research Laboratory, US Environmental Protection Agency, 109 T.W. Alexander Dr., Research Triangle Park, NC 27711, USA
[e] Russian Scientific Center "Kurchatov Institute", 1 Kurchatov Square, Moscow, 123182, Russia
[f] Institute of Environmental Physics, University of Bremen, 1 Otto Hahn Allee, Bremen, D-28334, Germany

ARTICLE INFO

*Article history:*
Received 3 December 2008
Received in revised form
5 March 2009
Accepted 6 March 2009

*Keywords:*
Radiative transfer
Plane albedo
Natural waters
Numerical solutions
Analytical solutions
Strongly anisotropic phase function

ABSTRACT

Several numerical and analytical solutions of the radiative transfer equation (RTE) were compared for plane albedo in a problem of solar light reflection by sea water. The study incorporated the simplest case—a semi-infinite one-dimensional plane—parallel absorbing and scattering homogeneous layer illuminated by a monodirectional light beam. Inelastic processes (such as Raman scattering and fluorescence), polarization and air–water surface refraction–reflection effects, were not considered. Algorithms were based on the invariant imbedding method and two different variants of the discrete ordinate method (DOM). Calculations were performed using parameters across all possible ranges (single-scattering albedo $\omega_0$ and refracted solar zenith angle $\theta_1$), but with a special emphasis on natural waters. All computations were made for two scattering phase functions, which included an almost isotropic Rayleigh phase function and strongly anisotropic double-peaked Fournier–Forand–Mobley phase function. Models were validated using quasi-single-scattering (QSSA) and exponential approximations, which represent the extreme cases of $\omega_0 \to 0$ and $\omega_0 \to 1$, respectively. All methods yielded relative differences within 1.8% for modeled natural waters. An analysis of plane albedo behavior resulted in the development of a new extended QSSA approximation, which when applied in conjunction with the extended Hapke approximation developed earlier, resulted in a maximum relative error of 2.7%. The study results demonstrated that for practical applications, the estimation of inherent optical properties from observed reflectance can best be achieved using an extended Hapke approximation.



## 1. Introduction

A solution of the radiative transfer equation (RTE) for reflectance as a function of inherent optical properties (IOPs) for an absorbing and scattering medium with the inclusion of lighting geometry is an important issue for numerous

☆ *Notice*: The US Environmental Protection Agency funded and partially conducted the research described in this paper. Although this work was review by EPA and has been approved for publication, it may not necessarily reflect official Agency policy. Mention of any trade names or commercial products does not constitute endorsement or recommendation for use.

* Corresponding author. Tel.: +1 919 541 3071; fax: +1 919 541 9420.
*E-mail addresses:* sokoletsky.leonid@epa.gov, sokoletsky.leonid@gmail.com (L.G. Sokoletsky).

0022-4073/$ - see front matter © 2009 Elsevier Ltd. All rights reserved.
doi:10.1016/j.jqsrt.2009.03.006

technological and environmental applications. One important ongoing research application is the use of remote sensing (RS) to monitor natural waters using both satellites and aircraft-based systems. Various methods for the RTE solution are currently being studied in an effort to develop an optimal solution for different natural water applications [1–5].

Only under conditions of strong scattering or absorption one can get accurate analytical solutions for different reflectance types (e.g. reflection function, plane and spherical albedos) [6,7]. However, to obtain an accurate RTE solution, when both scattering and absorption are important factors, different numerical methods must be applied. Stochastic (Monte Carlo) simulations can provide good results, but they are computationally intensive for optically thick media under complicated scattering phase functions (non-monotonic and/or strongly peaked), and often result in statistical fluctuations for computed values [8]. This is especially critical when solving the inverse optical problem (i.e., decomposition of measured radiance or reflectance into IOPs). Thus, different techniques are of interest [9] for theoretical and applied purposes to reduce computational expenses. For example, the iterative solution of the Ambartsumian's nonlinear integral equation (NIE) (another name of this method is invariant imbedding, IIM) [10], defines reflectance without calculating within-layer solution. Independent approximations for both the singular (strongly variable) and regular (slowly variable) parts of the solution can also be effective [11].

Although accurate numerical methods based on IIM and discrete ordinates (DOM) techniques are available [10,12], model comparisons between these methods have been limited to consideration of underwater radiance and irradiance [8] or reflection function [13]. Such comparisons show that both the IIM and DOM methods yield equal accuracy quantities; however, different Monte Carlo methods may generate upwelling values with significant error. For example, under idealized natural waters conditions (no atmosphere, incident solar zenith angle $\theta_0 = 60^\circ$, flat air–water surface, homogeneous and infinitely deep water column, and average-particle scattering phase function [14]), the average error of the nadir-viewing upwelling radiance at the water surface level computed by the Monte Carlo methods was approximately 6% [8].

A comparison of reflection function calculated by IIM [15] with that by DOM [16] also demonstrated [13] an excellent agreement between these two methods (excepting the rainbow region at phase angle range between $10^\circ$ and $15^\circ$) for semi-infinite layers of almost non-absorbing 200 μm spherical homogeneous particles with relative refractive indices 1.59 and strongly back-peaked scattering phase function.

The principal optical quantity investigated in this study was plane albedo. This optical property is important for ocean optics investigations because it can be considered as a component of diffuse or irradiance reflectance [17,18]. Plane albedo is a commonly measured quantity in experimental ocean optics that is typically measured by integrating spheres [19, p. 286] or by radiance sensors with calibrated plane albedo standards [20]. This optical property often called by the other names like "directional-hemispherical reflectance", "hemispherical reflectance", "flux reflectance", "diffuse reflectance of the surface, illuminated by the direct solar rays", "hemispherical albedo", or "black-sky albedo" [5,17–22]. We use the term "plane albedo" as more acceptable in publications on radiative transfer [5,7,9,22,23].

Only analytical approximations to the plane albedo have been compared previously [7,24,25]. The lack of comparisons between numerical methods for calculation of plane albedo in natural waters conditions represents a significant problem for the development of theoretically well-grounded *in situ* and RS aquatic optics algorithms. This study compares calculations of plane albedo according to three numerical approaches that include: (a) IIM [15]; (b) a combination of the DOM (for the regular part of RTE solution) and a small angle modification of a spherical harmonics method, MSH (for the singular anisotropic part of RTE solution) [11]; and (c) a version of DOM based upon a direct approximation of RTE [26].

The first and second methods take into account specific features of the solution being sought. That is, the NIE algorithm is intended for semi-indefinite plane-parallel layer, and DOM+MSH technique has been developed for the simulation of radiative fields in media with strongly peaked phase functions. The third method is direct as it is not based upon any assumptions on phase functions or the thickness of the medium. Additionally, we exploited different analytical approximations for plane albedo for verification of numerical solutions in extreme conditions.

To obtain a rigorous solution and avoid extraneous influence—the simplest case was studied—a semi-infinite one-dimensional plane-parallel absorbing and scattering homogeneous layer illuminated by a monodirectional light beam without regard for inelastic processes (e.g., Raman scattering and fluorescence), polarization and air–water surface refraction–reflection effects. To generalize a solution, we used all possible ranges of the single-scattering albedo $\omega_0 = b/c$ ($b$ and $c$ are the scattering and attenuation coefficients, respectively) and refracted angles $\theta_1$ (including angles greater than Brewster's angle) for our calculations. Also, we analyzed our results to account for the realistic optical conditions pertaining to natural waters. Specifically, we compared numerical solutions for the all possible angles $\theta_1 \in [0^\circ; 90^\circ]$ and $\omega_0 \in [0; 1]$ with a special emphasis on the natural waters [1,4] with $\theta_1 \in [0^\circ; 48.7^\circ]$ and $\omega_0 \in [0.1; 0.95]$.

The question of dependence of plane albedo on type of particulate scattering phase function was considered separately.

## 2. Background

### 2.1. Definitions and relationships

We consider the case of a sea water illuminated by collimated parallel beam that is incident on sea surface at angle $\theta_0$ with beam refracted at sea surface entering the water at an angle $\theta_1$ (Fig. 1). We accounted for a large optical thickness

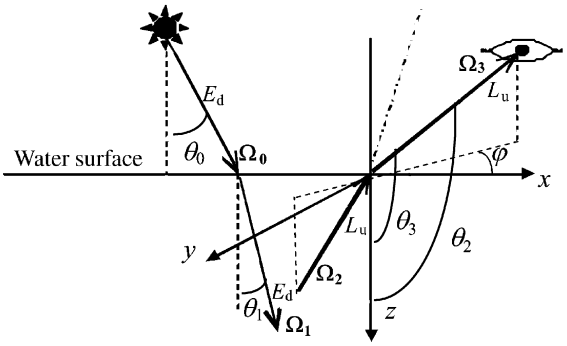


**Fig. 1.** A schematic geometry and symbols for incoming, refracted and reflected fluxes and angles.

$\tau^* = c(\Delta Z)$ ($\Delta Z$ is the geometrical thickness of plane-parallel layer), calm surface, and semi-infinite 1-D plane-parallel layers.

Radiative transport was simulated via transfer equation, written in the form [1–5,9,12,13,22,23]:

$$\mu_2 \frac{\partial L(\tau,\mu_2,\varphi_2)}{\partial \tau} = -L(\tau,\mu_2,\varphi_2) + \frac{\omega_0}{4\pi}\int_{-1}^{1} d\mu_1 \int_0^{2\pi} L(\tau,\mu_1,\varphi_1)p(\chi)\,d\varphi_1,$$
$$\tau \in (0,\infty), \quad \mu_2 \in (-1,1), \quad \varphi_2 \in (0,2\pi), \tag{1}$$

where solution $L$ defines unpolarized radiance at optical depth $\tau$ within the water layer. The scattering angle $\chi$ is related to the incident $(\mu_1,\varphi_1)$ and scattering $(\mu_2,\varphi_2)$ directions within the water by the geometrical relationship [7,8]:

$$\chi = \arccos[\mu_1\mu_2 + \sqrt{(1-\mu_1^2)(1-\mu_2^2)}\cos(\varphi_2-\varphi_1]}, \quad \mu_1 = \cos\,\theta_1, \quad \mu_2 = \cos\,\theta_2. \tag{2}$$

Eq. (1) contains two parameters. They are single scattering albedo $\omega_0$ and scattering phase function $p(\chi)$. The following boundary condition is defined just below the water surface (i.e. at the depth of 0+):

$$L(0+,\mu_2,\varphi_2)|_{\mu_2>0} = L_0\delta(\mu_2-\mu_1)\delta(\varphi_2), \tag{3}$$

where $\delta$ is the Dirac's delta function and $L_0$ is the incident beam radiance.

Far from the surface radiance is negligible as a result of absorption and multiple scattering processes:

$$L(\tau,\mu_2,\varphi_2) \to 0 \quad \text{for } \tau \to \infty. \tag{4}$$

The reflection function $R$ is defined [6,13,19,22,27] as the ratio of the intensity of light (radiance) reflected from a given turbid layer to the intensity of light reflected from the perfectly reflecting Lambertian surface for given incident beam direction $\mathbf{\Omega}_0$ (or for the given refracted beam direction $\mathbf{\Omega}_1$) and observation direction $\mathbf{\Omega}_2$ (or $\mathbf{\Omega}_3$) (Fig. 1). Thus, $R$ is determined via incident solar zenith angles $\theta_0$ (or $\theta_1$) for air (water), viewing nadir angles $\theta_2$ (or $\theta_3$) for water (air), the refracted azimuth angle $\varphi_1$ and viewing (in the water) azimuth angle $\varphi_2$.

$R$ is equal to 1 for Lambertian surface. For the water medium with any optical properties we can write $R$ in the form [13,19,22]:

$$R(\theta_1,\theta_2,\varphi_1,\varphi_2) = \frac{\pi}{\mu_1}\frac{L_u(\theta_2,\varphi_2)}{E_d^{dir}(\theta_1,\varphi_1)}, \tag{5}$$

where $E_d^{dir}$ is the incident direct (collimated) irradiance and $L_u$ is the upwelling radiance.

The plane albedo [6,19] $\Re$ just below the water surface is defined as the integral of the reflection function $R$:

$$\Re(\mu_1) = \frac{1}{\pi}\int_0^{2\pi} d\varphi_2 \int_{-1}^{0} R(\mu_1,\mu_2,\varphi_2)\mu_2\,d\mu_2. \tag{6}$$

Eq. (6) imposes a wide range for angles $\theta_1$ and $\theta_2$: [0°; 90°]. However, for situations of refraction at air–water surface, angles $\theta_1$ and $\theta_2$ are connected with the angles $\theta_0$ and $\theta_3$ through Snell's law of geometrical optics as

$$\theta_1 = \arcsin(\sin\,\theta_0/n_w), \quad \theta_2 = \arcsin(\sin\,\theta_3/n_w), \tag{7}$$

where $n_w$ is the refractive index of seawater. Thus, at $n_w = 1.330$, a common value for natural waters, the realistic range of $\theta_1$ and $\theta_2$ [0°; 48.7°] is limited by the Brewster's angle. Nevertheless, in Eq. (6) and henceforth we allow for the full range of $\mu_2$ [0; 1], to maintain generality in our algorithms and calculations.

Sokoletsky [18] has shown by comparing several radiative transfer approximations that a layer can be taken as an "optically thick" when optical thickness ($\tau_k$) for the diffuse attenuation coefficient ($K_d$) defined as $\tau_k \equiv K_d\Delta Z$ ($\Delta Z$ is the geometrical thickness of the layer) more than 4. $K_d$ may be approximated (within the framework of the quasi-single-scattering approximation, QSSA) as [28,29] $K_d = (a+b_b)/\mu_1$, where $a$ and $b_b$ are the absorption and backscattering coefficients, respectively. Using this expression, one can relate $\tau_k$ with a "classical" optical thickness for optically

homogeneous layer $\tau \equiv c\Delta Z$ by

$$\tau = \frac{\mu_1}{1-\omega_0 F}\tau_k, \tag{8}$$

where $F$ is the forward-scattering probability, defined as

$$F = \frac{1}{2}\int_0^{\pi/2} p(\chi)\,\sin\chi\, d\chi. \tag{9}$$

Our numerical computations carried out for FFM scattering phase function (see below) within turbid layer show that the value of $\tau_k = 4$ yielded a negative relative error of plane albedo (compared to plane albedo values computed for $\tau_k \gg 4$) and ranged from 0.0% to −0.3% at values of $\omega_0$ running from 0 to 0.995. However, values of errors sharply increased (approximately up to 8%) at further increasing $\omega_0$. We will give below (Section 3.3) an exact algorithm for estimation of optical thickness simulating the semi-infinite turbid layer used in the study.

### 2.2. Scattering phase functions

Although angle dependence $p(\chi)$ can be quite variable for natural waters [30], we considered only two phase functions. The first scattering phase function is the strongly forward-peaked Fournier–Forand–Mobley (FFM) phase function [14] that is close to scattering phase functions observed in ocean water [6] and has been proven to be applicable in natural waters [31]. This allowed for a comparison between different peak-forward phase functions (Section 4.3). An almost isotropic Rayleigh scattering phase function describing scattering by the water molecules [3] corresponds to the extreme case of minimal particulate matter, and was used for debugging the computer codes and to quantify the impact of $p(\chi)$ on computational accuracies.

The exact angular dependence for the Rayleigh $p(\chi)$ (Fig. 2) may be written as follows:

$$p_{Rayleigh}(\chi) = (3/4)(1+\cos^2\chi), \tag{10}$$

and it yields $F = 0.5$ and the asymmetry parameter $g = 0$, where $g$ is defined as

$$g = \frac{1}{2}\int_0^{\pi} p(\chi)\,\sin\chi\,\cos\chi\, d\chi. \tag{11}$$

The exact expression for the particulate FFM scattering phase function is given by [14]

$$p_{FFM}(\chi) = \frac{j(1-\delta)-(1-\delta^j)+2[\delta(1-\delta^j)-j(1-\delta)]/(1-\cos\chi)}{(1-\delta)^2\delta^j} + \frac{(1-\delta_{180}^j)(3\cos^2\chi-1)}{4(\delta_{180}-1)\delta_{180}^j}, \tag{12}$$

where

$$j = \frac{3-J}{2}, \quad \delta = \frac{2(1-\cos\chi)}{3(n-1)^2}, \quad J = 3 + \frac{n-1.01}{0.1542}. \tag{13}$$

Here $n$ is the real index of refraction of the particles and $J$ is the slope parameter of the particle hyperbolic (Junge-type) distribution. Importantly, at $n = 1.10$, $p_{FFM}(\chi)$ corresponded well to the Petzold's average-particle phase function observed in San Diego Harbor [14].

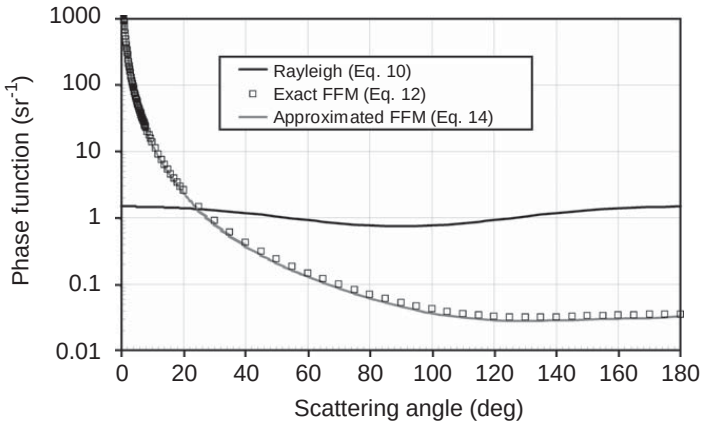


**Fig. 2.** Three scattering phase functions, two of which: Rayleigh (solid line) and FFM (squares) were determined by Fourier–Legendre series, Eq. (14) and have been selected for analysis. The corresponding "exact FFM" phase function (wavy line) defined in [14] has parameters of particle refractive index $n = 1.10$ and the slope parameter of Junge-type distribution $j = 3.5835$.

The phase functions in the IIM and DOM+MSH methods were set by the finite Fourier–Legendre series, namely:

$$p(\chi) = \sum_{i=0}^{i_{\max}} a_i P_i(\cos\ \chi), \tag{14}$$

where $a_i$ and $P_i(\cos\chi)$ are Fourier–Legendre coefficients [32] and Legendre polynomials [33], respectively, derived to obey the normalization condition:

$$\frac{1}{2}\int_0^{\pi} p(\chi)\ \sin\ \chi\, d\chi = 1. \tag{15}$$

The Rayleigh phase function (10) can be exactly expressed by only two terms of the Fourier–Legendre series in the form: $p_{\text{Rayleigh}}(\chi) = 1+P_2(\cos\chi)$, yielding $F = 0.5$ and $g = 0$.

Generally, the more asymmetric the phase function, greater the number of terms to achieve the required accuracy. Taking into account that $p_{\text{FFM}}(\chi)$ runs six orders of magnitude (Fig. 2) with two peaks (forward and backward), it was difficult to accurately express this $p(\chi)$ over all angles by the Fourier–Legendre series. Nevertheless, we used Eq. (14) with $L = 1998$ and mathematically derived values of $a_i$ for a representation of $p_{\text{FFM}}(\chi)$ (Fig. 2). A $p_{\text{FFM}}(\chi)$ was defined to derive parameters of $g = 0.9377$, $F = 0.98168$, compared with $g = 0.9300$, $F = 0.98170$ for the "exact" FFM phase function, defined by Eq. (12).

A comparison between the approximated FFM and exact FFM phase functions was realized by the root-mean-square percentage difference calculated for the scattering angles weighted by the sines and in the angular scattering ranges as recommended by Mobley et al. [14]. This yielded values of 1.8%, 1.3%, and 1.9% over 5–90°, 90–180° and 5–180°, respectively. Comparison shows that the FFM phase function approximated by a Fourier–Legendre series is closer to the exact FFM ($n = 1.10$) than the phase functions of different types considered by Mobley et al. [14]. Additionally, the approximated FFM did not have a singularity at the zero scattering angles, as with the exact FFM, and could be recommended for natural water optics investigations.

## 3. Methods

Analytical approximations to the plane albedo were compared with numerical solutions (Section 4.1). These approximations lead to the exact solution at $\omega_0 \to 0$ and $\omega_0 \to 1$, respectively. The analysis permitted the development of a new approximation for the plane albedo termed "extended QSSA" (Section 4.2). The dependence of plane albedo on particulate scattering phase function is considered in Section 4.3.

Numerous difficulties were encountered in numerical solving the RTEs. First, was the need to deal with radiation fields in the finite layer with large variations over spatial variable $\tau$. Second, we had to simulate complex scattering according to FFM double-peaked phase function. Lastly, the need to account for the high spatial boundary gradients for a small refracted angle $\theta_1$. To avoid numerical errors caused by these difficulties we used a feature of the medium with conservative scattering: $\Re\,(\omega_0 = 1) = 1$. This is logical since all radiation entered into completely scattering medium could leave the layer after infinite travel time. This result may also be derived analytically, if to integrate Eq. (1) over all variables $\tau$, $\mu$, $\varphi$ using boundary conditions (3) and (4) and definition (6).

### 3.1. Iterative solution of the Ambartsumian's NIE ("invariant imbedding method, IIM")

Instead of RTE (Eq. (1)), a NIE [10] by Ambartsumian (1943) for radiance reflected by a semi-infinite plane-parallel layer with arbitrary phase function $p(\chi)$ and the single scattering albedo $\omega_0$ was solved. This equation was based on the "principle of invariant imbedding", derived firstly for non-absorbing (transparent) layers by A.J. Fresnel in 1821 and then by G.G. Stokes in 1862 for the absorbing (opaque) layers. Further, this principle was extended for different conditions by numerous researches such as Neumann, Schmidt, Shuster, Wien-Harms, Ambartsumian, Sobolev, Chandrasekhar, Tuckerman, Bellman, Wing and Preisendorfer [34–37].

Ambartsumian's equation does not simulate radiative fields within a layer because it excludes optical thickness $\tau$, thus reducing computational requirements. Previous results have demonstrated [10] that a reflection function obtained via RTE converges to a NIE solution as $\tau \to \infty$. We used the open source code developed by Mishchenko et al. [15] for the solution of Ambartsumian's equation.

The computational technique here is based on the expansion of the reflection function and also the phase function in Fourier series with respect to the azimuth. The NIE for the $m$-th harmonic of the reflection function $R_m(\mu_1,\mu_2,\varphi_2)$ is written in the following form [15]:

$$\begin{aligned} R_m(\mu_1,\mu_2,\varphi_2,\tau\to\infty) = \omega_0[&F_m(\mu_1,\mu_2,\varphi_2) + \Phi_m(\mu_1,\mu_2,\varphi_2) + \Theta_m(\mu_1,\mu_2,\varphi_2) \\ &+ \Psi_m(\mu_1,\mu_2,\varphi_2)], \end{aligned} \tag{16}$$

where

$$F_m(\mu_1,\mu_2,\varphi_2)=\frac{P_m(\mu_1,-\mu_2,\varphi_2)}{4(\mu_1+\mu_2)}, \tag{17}$$

$$\Phi_m(\mu_1,\mu_2,\varphi_2)=\frac{\mu_1}{2(\mu_1+\mu_2)}\int_0^1 P_m(\mu_2',\mu_2,\varphi_2)R_m(\mu_1,\mu_2',\varphi_2)\,d\mu_2', \tag{18}$$

$$\Theta_m(\mu_2,\mu_1,\varphi_2)=\frac{\mu_2}{2(\mu_1+\mu_2)}\int_0^1 P_m(\mu_1,\mu_2',\varphi_2)R_m(\mu_2',\mu_2,\varphi_2)\,d\mu_2', \tag{19}$$

$$\Psi_m(\mu_1,\mu_2,\varphi_2)=\frac{\mu_1\mu_2}{\mu_1+\mu_2}\int_0^1 d\mu_2''\int_0^1 P_m(\mu_2'',-\mu_2',\varphi_2)R_m(\mu_2',\mu_2,\varphi_2)R_m(\mu_1,\mu_2'',\varphi_2)\,d\mu_2'. \tag{20}$$

Here $P_m\ (\mu_1,\mu_2,\varphi_2)$ is the $m$-th Fourier component of the phase function as it is described in detail by Mishchenko et al. [15]. Because ocean waters are weakly reflecting medium and the influence of multiple light scattering represented by integrals in Eq. (16) is rather weak, the NIE can be solved using the method iterations. In the first iteration, only the first term in Eq. (16) responsible for the first-order scattering is used.

### 3.2. Combined discrete ordinate and a modified spherical harmonics ("DOM+MSH") method

This method deals with the layer of definite (but large enough to ensure simulations of semi-infinite layers) optical thickness $\tau$ and was developed for modeling radiation fields in strongly anisotropic media with singular sources, where the RTE solution contains singularities. It is based on decomposition of the solution into the sum of the following two components [11]:

$$L(\tau,\mu_2,\varphi_2)=L_{SA\text{-}SHM}(\tau,\mu_2,\varphi_2)+\tilde{L}(\tau,\mu_2,\varphi_2). \tag{21}$$

The first component, $L_{SA\text{-}SHM}\ (\tau,\mu_2,\varphi_2)$, contains all the singularities of the exact solution of RTE and is defined as a solution of RTE in a small-angle (SA) modification (in the Goudsmit–Saunderson form [38]) of a spherical harmonics method (SHM):

$$L_{SA\text{-}SHM}(\tau,\mu_2,\varphi_2)=\sum_{i=0}^{\infty}\exp\left\{-\frac{[1-4\pi\omega_0 a_i/(2i+1)]\tau}{\mu_1}\right\}P_i(\mu_2), \tag{22}$$

where $a_i$ and $P_i$ are Fourier–Legendre coefficients and Legendre polynomials taken as in Eq. (14).

The latter component is the remaining part of the solution, which conforms to conditions:

$$\tilde{L}(0,\mu_2,\varphi_2)|_{\mu_2>0}=0,\quad \tilde{L}(\tau,\mu_2,\varphi_2)|_{\mu_2<0}=-L_{SA\text{-}SHM}(\tau,\mu_2,\varphi_2), \tag{23}$$

of the RTE written in the form:

$$\mu_2\frac{\partial\tilde{L}(\tau,\mu_2,\varphi_2)}{\partial\tau}=-\tilde{L}(\tau,\mu_2,\varphi_2)+\frac{\omega_0}{4\pi}\int_{-1}^{1}d\mu_1\int_0^{2\pi}\tilde{L}(\tau,\mu_1,\varphi_1)p(\chi)\,d\varphi_1+F(\tau,\mu_2,\varphi_2), \tag{24}$$

where source $F(\tau,\mu_2,\varphi_2)$ is residual of RTE in approximation $L_{SA\text{-}SHM}(\tau,\mu,\varphi_2)$:

$$\begin{aligned}F(\tau,\mu_2,\varphi_2)=&-\mu_2\frac{\partial L_{SA\text{-}SHM}(\tau,\mu_2,\varphi_2)}{\partial\tau}-L_{SA\text{-}SHM}(\tau,\mu_2,\varphi_2)\\&+\frac{\omega_0}{4\pi}\int_{-1}^{1}d\mu_1\int_0^{2\pi}L_{SA\text{-}SHM}(\tau,\mu_1,\varphi_1)p(\chi)\,d\varphi_1.\end{aligned} \tag{25}$$

This function is determined using the addition theorem for Legendre polynomials:

$$F(\tau,\mu_2,\varphi_2)=\sum_{m=-\infty}^{\infty}\sum_{k=0}^{\infty}F_k^m(\tau)Q_k^m(\mu_2)\,e^{im\varphi_2}, \tag{26}$$

where

$$\begin{aligned}F_k^m(\tau)=&\frac{1}{\mu_1}[\sqrt{(k+1)^2-m^2}b_{k+1}Q_{k+1}^m(\mu_1)Z_{k+1}(\tau)+\sqrt{k^2-m^2}b_{k-1}Q_{k-1}^m(\mu_1)Z_{k-1}(\tau)]\\&-\frac{2k+1}{4\pi}b_kQ_k^m(\mu_1)Z_k(\tau),\quad b_k=1-4\pi\omega_0a_k/(2k+1),\end{aligned}$$

$$Z_k(\tau)=\exp\left\{-\frac{[1-4\pi\omega_0a_k/(2k+1)]\tau}{\mu_1}\right\}. \tag{27}$$

Here $Q_l^n(\mu_1)=\sqrt{(l-n)!/(l+n)!}P_l^n(\mu_1)$, $P_l^n(\mu_1)$, $P_k(\mu_1)$—semi-normalized, associated, and classical Legendre polynomials, correspondingly.

By decomposing $L(\tau,\mu_2,\varphi_2)$ over azimuth $\varphi_2$:

$$L(\tau,\mu_2,\varphi_2)=\sum_{m=-\infty}^{\infty} C^m(\tau,\mu_2)\,e^{im\varphi_2}, \tag{28}$$

and taking into account relation (27) and orthogonality of spherical harmonics $e^{im\varphi_2}$, we obtain equations for expansion coefficients $C^m(\tau,\mu_2)$:

$$\mu_2\frac{\partial C^m(\tau,\mu_2)}{\partial\tau}=-C^m(\tau,\mu_2)+\sum_{k=0}^{\infty}F_k^m(\tau)Q_k^m(\mu_2) +\frac{1}{2}\omega_0\sum_{k=m}^{N}a_kQ_k^m(\mu_2)\int_{-1}^{1}Q_k^m(\mu_1)C^m(\tau,\mu_1)\,d\mu_1. \tag{29}$$

Then replacing the integral on the right side of these equations via Gauss quadrature we find a linear system of equations:

$$\overleftrightarrow{M}\frac{\partial\vec{C}^m(\tau)}{\partial\tau}=-\vec{C}^m(\tau)+\vec{F}^m(\tau)+\overleftrightarrow{S}\,\vec{C}^m(\tau), \tag{30}$$

where $\vec{C}^m=\{C_i^m\}$ is the vector being sought, $\overleftrightarrow{M}=Diag(\mu_2^i)$ is diagonal matrix, and matrices $\vec{F}^m(\tau)$ and $\overleftrightarrow{S}$ are defined by expressions

$$\vec{F}^m(\tau)=\left\{\sum_{k=m}^{\infty}F_k^m(\tau)Q_k^m(\mu_2^i)\right\},\quad \overleftrightarrow{S}=\left\{2\pi w_j\sum_{k=m}^{\infty}a_kQ_k^m(\mu_2^i)Q_k^m(\mu_2^j)\right\}, \tag{31}$$

where $\mu_2^j$ are the roots of Legendre polynomials $P_N(\mu_2^j)=0$, $w_j$ are the weights of Gauss quadrature of the order $N$.

A system of linear differential equations (30) with constant coefficients has an analytical solution in the form of a matrix exponent [11,39,40]. This spherical harmonic system is not consistent with RTE boundary conditions (1), and conditions of the Mark type [41] were used to represent a unique approximation. Using Mark's boundary conditions along with the other well-known tools of RTE solution (i.e., SHM and DOM) have demonstrated efficiency when some singularities occur [11,39,40].

Conditionality of a matrix of system (30) quickly deteriorates with increasing layer's optical thickness. To alleviate this problem, a scale transformation [39] was used that led to an expression with exponents with negative degrees $\tau$ to derive a solution for semi-infinite layer. In Eqs. (21)–(31), optical thickness $\tau$ may be any value, but for the method under consideration, $\tau$ has been taken as infinity for all calculations using Matlab software with a constant Inf (“infinity”).

### 3.3. Discrete ordinate method, DOM (“RADUGA's Method”)

The code RADUGA-5.1 (see [26]) has been developed to solve RTE in 1-, 2-, and 3-D regions via DOM by a parallel supercomputer (MVS-1500BM) [42] of the Russian Academy of Sciences containing 1148 processors (200 were actually used), under general assumptions on source and media properties. The method here incorporated direct replacement of RTE by algebraic equations system based on the following:

1. We consider problem expressed by Eqs. (1)–(4) for a finite layer of very large optical thickness $\tau^*$ defined by condition $\tau_k^*=5$ for $\omega_0<0.995$ and $\tau^*=350$ for $\omega_0\geqslant 0.995$. Such a choice is based on numerical experiments with different optical thicknesses. A layer of optical thickness $\tau^*$ may be considered as the semi-infinite layer, if increasing of $\tau^*$ by 10 changes a plane albedo by 0.001.

2. We decomposed the solution into unscattered radiance $L_{unsc}(\tau,\mu_2,\varphi_2)$ and scattered radiance $L_{sc}(\tau,\mu_2,\varphi_2)$:

$$L(\tau,\mu_2,\varphi_2)=L_{unsc}(\tau,\mu_2,\varphi_2)+L_{sc}(\tau,\mu_2,\varphi_2). \tag{32}$$

Each of these functions were determined using a corresponding transport problem:

$$\begin{aligned}&\mu_2\frac{\partial I_{unsc}(\tau,\mu_2,\varphi_2)}{\partial\tau}+L_{unsc}(\tau,\mu_2,\varphi_2)=0,\quad \tau\in(0+,\tau^*),\ \ \mu_2\in(-1,1),\\ &\varphi_2\in(0,2\pi),\quad L_{unsc}(0+,\mu_2,\varphi_2)|_{\mu_2>0}=L_0\delta(\mu_2-\mu_1)\delta(\varphi_2),\\ &L_{unsc}(\tau^*,\mu_2,\varphi_2)|_{\mu_2<0}=0,\end{aligned} \tag{33}$$

$$\begin{aligned}&\mu_2\frac{\partial L_{sc}(\tau,\mu_2,\varphi_2)}{\partial\tau}=-L_{sc}(\tau,\mu_2,\varphi_2)+\frac{\omega_0}{4\pi}\int_{-1}^{1}d\mu_1\int_0^{2\pi}[L_{unsc}(\tau,\mu_1,\varphi_1)+L_{sc}(\tau,\mu_1,\varphi_1)]p(\chi)\,d\varphi_1,\\ &\tau\in(0+,\tau^*),\quad \mu_2\in(-1,1),\ \ L_{sc}(0+,\mu_2,\varphi_2)|_{\mu_2<0}=0,\ \ L_{sc}(\tau^*,\mu_2,\varphi_2)|_{\mu_2>0}=0.\end{aligned} \tag{34}$$

Unscattered radiance $L_{unsc}(\tau,\mu_2,\varphi_2)$ was determined analytically and a grid method was used for scattered radiance $L_{sc}(\tau,\mu_2,\varphi_2)$.

3. We introduced a uniform angular grid over angular variable $\mu_2$ and $\varphi_2$. The grid was formed by pairs $(\mu_2^k, \varphi_2^k)$ and identical weights $w_k \equiv w$, $k = 1, \ldots, K$, and permitted replacing the scattering integral with a quadrature sum:

$$\int_{-1}^{1} d\mu' \int_0^{2\pi} L_{sc}(\tau, \mu_2, \varphi_2) p(\chi)\, d\varphi_2 \cong \sum_{k'} L_{sc}^{k'}(\tau) w_{k'} p_{k,k'}, \tag{35}$$

where symbol $L_{sc}^{k'}(\tau)$ stands for $L_{sc}(\tau, \mu_{k'}, \varphi_{k'})$, the multiplier $p_{k,k'}$ was defined via values of a phase function for scattering angles $\chi$, corresponding to scattering event from direction $(\mu_{k'}, \varphi_{k'})$ to direction $(\mu_k, \varphi_k)$. Each value of $p_{k,k'}$ was calculated via a high order Gauss quadrature formula based upon a piece-wise linear approximation of a phase function via its value in nodes of some grid over scattering angle $\chi$. A high order Gauss quadrature formula accurately takes into consideration the complicated twice-peaked phase function. Note, because the scattering matrix does not depend on $\omega_0$ and $\mu_1$, it was calculated first.

4. We introduced a grid over spatial variable $\tau$ by nodes $\tau_{j+1/2}$:

$$0 = \tau_{1/2} < \tau_{3/2} < \cdots < \tau_{j-1/2} < \tau_{j+1/2} < \cdots < \tau_{j+1/2} = \tau^* \tag{36}$$

and replaced the left side of RTE (Eq. (1)) by algebraic relations, containing a solution at layer boundaries $L_{sc}^k(\tau_{1/2})$ and $L_{sc}^k(\tau_{j+1/2})$ and mean solution values in cells $[\int_{\tau_{j-1/2}}^{\tau_{j+1/2}} L_{sc}^k(\tau)\, d\tau]/(\tau_{j+1/2} - \tau_{j-1/2})$ using a non-uniform spatial grid refined in the vicinity of the extremes of the solution.

5. We composed an algebraic equation system approximating RTE solution as

$$\hat{S}\vec{L} = \hat{T}\vec{L} + \vec{Q}, \tag{37}$$

where vectors $\vec{L}$ and $\vec{Q}$ contain required grid function values and source values, correspondingly, $\hat{S}$ and $\hat{T}$ are some matrices.

6. To solve this algebraic system we applied a two-step iterative technique. The first step incorporated a source iteration method:

$$\hat{S}\vec{L}^{it+1/2} = \hat{T}\vec{L}^{it} + \vec{Q}, \tag{38}$$

and accelerating correction was added to the solution at the second step:

$$\vec{L}^{it+1} = \vec{L}^{it+1/2} + \vec{\varepsilon}^{it+1/2}. \tag{39}$$

Correction $\vec{\varepsilon}^{it+1/2}$ is defined as the approximate solution of equation for error of function $\vec{L}^{it+1/2}$:

$$\hat{S}(\vec{L} - \vec{L}^{it+1/2}) = \hat{T}(\vec{L} - \vec{L}^{it+1/2}) + \hat{T}(\vec{L}^{it+1/2} - \vec{L}^{it}). \tag{40}$$

We used an approximate solution for this equation based on a linear approximation over $\mu_k$:

$$\varepsilon_k(\tau_{j+1/2}) = \varphi^0(\tau_{j+1/2}) + 3\varphi^1(\tau_{j+1/2})\mu_k, \tag{41}$$

where functions $\varphi^0(\tau_{j+1/2})$ and $\varphi^1(\tau_{j+1/2})$ were derived from the two equalities obtained by averaging Eq. (39) over $\mu_k$ and $\varphi_k$ with weights 1 and $\mu_k$, respectively.

This acceleration technique resulted in convergence within 35 iterations. The simplifications accounted for the particularities of a desired solution generally used in other numerical methods but not previously incorporated into the RADUGA method. Thus, it can be applied for the calculation of radiation fields with arbitrary features. A Fourier–Legendre series (Eq. (14)) to a phase function was not used in this algorithm. Instead, we used an approximation to the phase function $p(\chi)$, based on values in 10 801 nodes over scattering angle $\theta$. This technique is stable and also supports the solution for RTE under the exact phase function $p(\chi)$ [43].

### 3.4. Quasi-single-scattering approximation (QSSA)

An equation expressing reflection function $R$ as a function of IOPs in the frame of QSSA had been initially supposed by Gordon [28]. The QSSA is based on the premise that $p(\chi)$ is highly peaked in the forward direction in natural waters, so most of the scattered light remains in the beam, and all of the losses result from absorption and backscattering. Also it is assumed that the probability of photon absorption is great.

A derivation of equations for the reflection function $R$ and for the plane albedo $\Re$ for QSSA was presented by Anikonov and Ermolaev [44] and Kokhanovsky and Sokoletsky [7], respectively:

$$R(\omega_0, F, p(\chi), \mu_1, \mu_2) = \frac{\omega_0}{4(1 - \omega_0 F)} \frac{p(\chi)}{\mu_1 + \mu_2}, \tag{42}$$

$$\Re(\omega_0, F, a_i, \mu_1) = \frac{\omega_0}{2(1 - \omega_0 F)} \sum_{i=0}^{L} (-1)^i a_i P_i(\mu_1) Q_i(\mu_1), \tag{43}$$

where $F$, $a_i$ and $P_i$ represent the forward-scattering probability, Fourier–Legendre coefficients and Legendre polynomials, respectively, as defined above; $Q_i$ is the function defined as

$$Q_i(\mu_1) = \int_0^1 P_i(\mu_2)(\mu_1+\mu_2)^{-1}\mu_2\, d\mu_2. \tag{44}$$

Further simplification of QSSA may be obtained, if to explore $p(\chi)$ with the constant scattering in backward hemisphere (i.e. at scattering angles from $\pi/2$ to $\pi$). In this case, from Eq. (9) follows that $p(\chi) = 2(1-F)$. Substituting this result in Eq. (42) we get

$$R(\omega_0, F, \mu_1, \mu_2) = \frac{1}{2(\mu_1+\mu_2)}\frac{1-F}{1-\omega_0 F}. \tag{45}$$

Eq. (45) directly shows that reflection function increases with increasing $\omega_0$ and decreases with $F$, $\mu_1$ and $\mu_2$. Keeping a relationship between $R$ and $\Re$ (Eq. (6)) in mind it is easy to derive similar conclusions about the plane albedo. Also note that at $\omega_0 \to 0$ or $F \to 0$, Eqs. (42), (43) and (45) converted to the form of the single-scattering approximation [13].

Different phase functions with the asymmetry parameter $g \in (0.85; 0.96)$ [7] Fig. 3b and c have yielded a relative error $|\delta|$of QSSA for the plane albedo smaller than 11% at $\omega_0 < 0.7$ and $\theta_0 \in [0^\circ; 70^\circ]$ comparing with the IIM method; it achieve $|\delta| = 0\%$ at $\omega_0 \to 0$ and any phase function. However, additional calculations [6] indicated that for a phase function with $g = 0.6962$ and $F = 0.9411$, QSSA has a maximal error $\delta = -35\%$ for $\theta_0 \in [0^\circ; 18^\circ]$

### 3.5. Exponential approximation (EA)

We use an EA in the form described in [7], Eq. (16):

$$\Re(s, \mu_1) = \exp\left[-\frac{4\sqrt{3}}{7}(1+2\mu_1)s\right], \tag{46}$$

where $s$ is the Hulst's similarity parameter [6,23] defined by

$$s = \sqrt{\frac{1-\omega_0}{1-g\omega_0}}. \tag{47}$$

Eq. (46) leads to the similar conclusions with respect to $\Re$ as in the case of QSSA approximation, namely, increasing $\Re$ with increasing $\omega_0$ and decreasing with $g$ (or, equivalently, with $F$) and $\mu_1$. An accuracy $|\delta|$of EA compared to an IIM method has been estimated (see [7], Fig. 2) to be $< 10\%$ at $s < 0.45$ (i.e., at $\omega_0 > 0.80$ or $\omega_0 > 0.98$ at $g = 0$ or 0.9377, respectively) and any incoming angle; it achieves $|\delta| = 0\%$ at $\omega_0 \to 1$ and any phase function.

## 4. Results

### 4.1. Verification of existing numerical and analytical methods

Three numerical methods were used to derive plane albedo $\Re$ from Eqs. (1) to (4) with Rayleigh and FFM scattering phase functions for different values of single-scattering albedo $\omega_0$ and cosine of the refracted angle just below the surface $\mu_1$. Fig. 3 presents the results of calculations by numerical methods (IIM and DOM+MSH) and analytical methods (extended

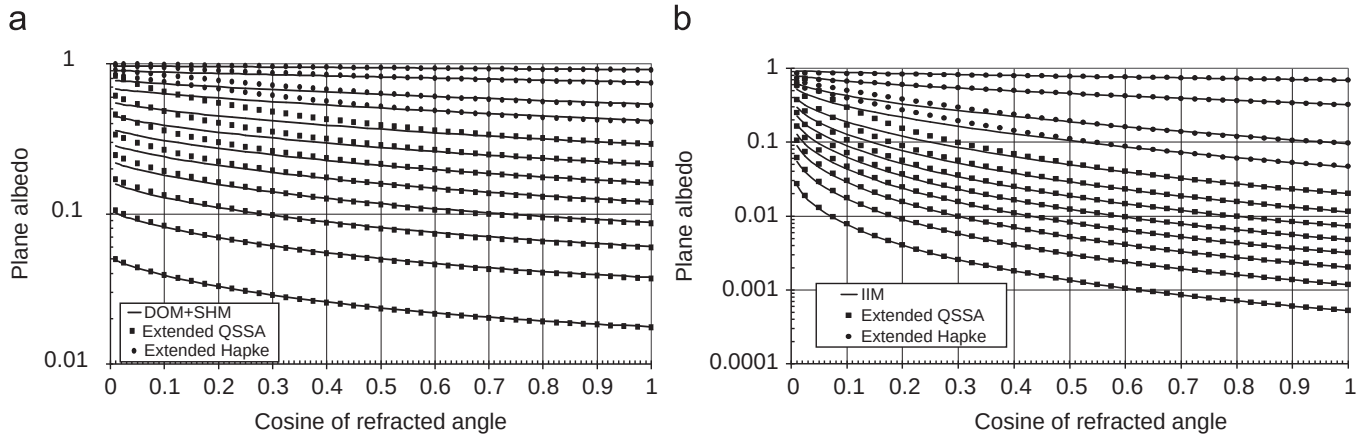


**Fig. 3.** Plane albedo for the Rayleigh (a) and FFM (b) scattering phase functions calculated by numerical methods (solid lines) for the following single-scattering albedo $\omega_0$ values: 0.1, 0.2, 0.3, 0.4, 0.5, 0.6, 0.7, 0.8, 0.9, 0.95, 0.99, and 0.999 (from the bottom to up); extended QSSA (squares) for $\omega_0 \leqslant 0.8$ and extended Hapke approximation (circles) for $\omega_0 > 0.8$.

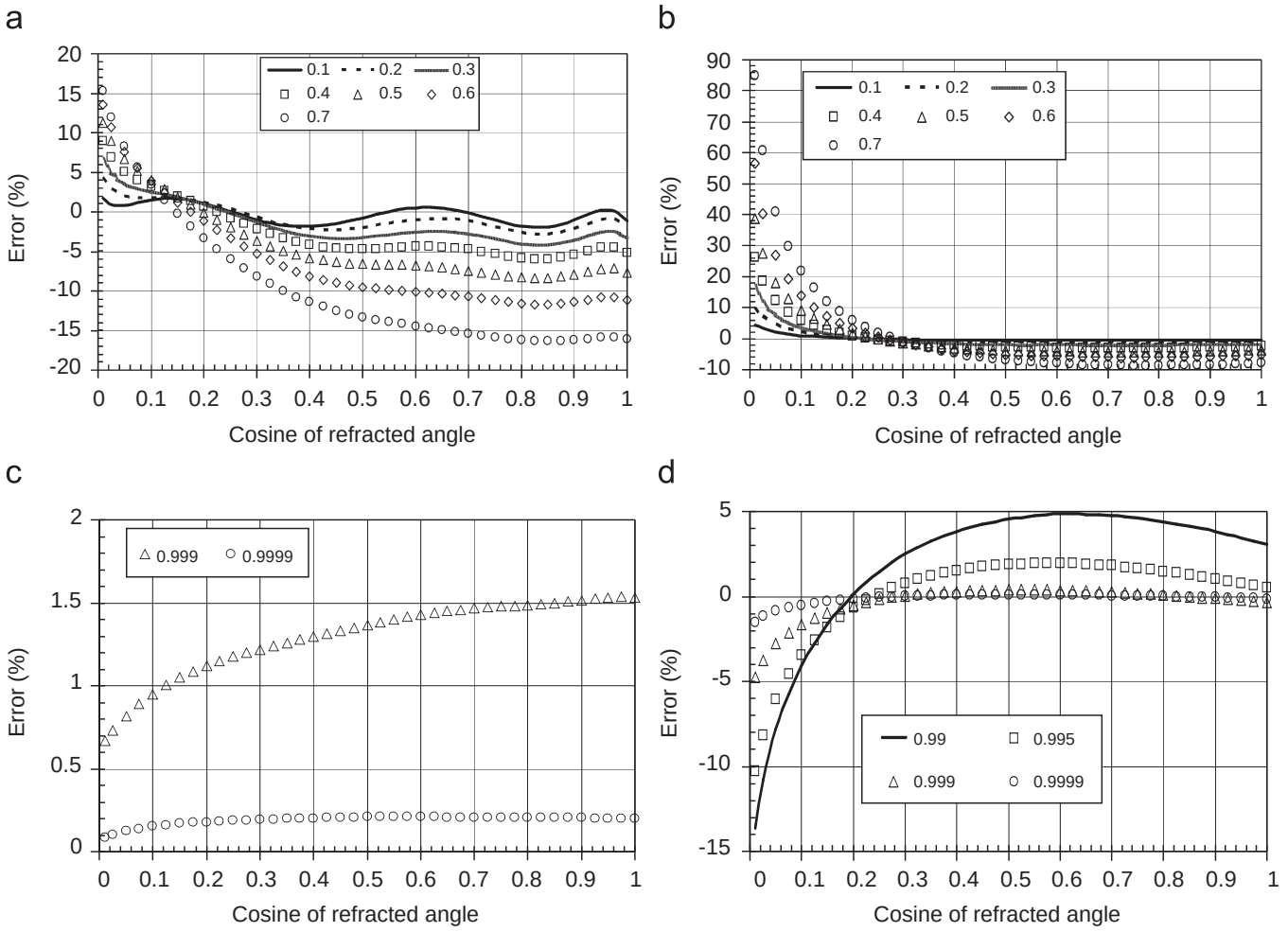


**Fig. 4.** Errors of QSSA (a, b) and EA (c, d) approximations vs. IIM method for Rayleigh (a, c) and FFM (b, d) scattering phase functions.

QSSA and extended Hapke) for Rayleigh and FFM phase functions. Both phase functions yield similar qualitative results: $\Re$ increases with increasing $\theta_1$ and $\omega_0$. However, quantitative predictions for $\Re(\omega_0, \theta_1)$ are highly dependent on phase function form.

For Rayleigh phase function, albedo angular dependence (Fig. 3a) was much flatter than for strongly forward-scattering FFM phase function (Fig. 3b). Fig. 4 shows relative errors between plane albedo approximations and IIM method for Rayleigh (Fig. 4a and c) and FFM (Fig. 4b and d) phase functions. Fig. 4(a and b) demonstrates how calculations performed using IIM matched with a QSSA approximation and Fig. 4(c and d) illustrates comparisons with EA approximation. The general tendencies illustrated by these plots include: (a) smaller errors for $p_{FFM}(\chi)$ than for $P_{Rayleigh}(\chi)$ for the QSSA approximation; (b) smaller errors for $P_{Rayleigh}(\chi)$ than for $p_{FFM}(\chi)$ for EA approximation; (c) decreasing divergence between numerical methods and QSSA at decreasing $\omega_0$ and between numerical methods and EA at increasing $\omega_0$ and (d) the errors of QSSA and EA generally larger at small values of $\omega_1$.

The result (c) may be strengthened: calculated errors of $\Re$ tend to zero at $\omega_0 \to 0$ and $\omega_0 \to 1$ comparing with QSSA and EA approximations, respectively. The results (a)–(c) may be expressed in terms of only similarity parameter $s$, namely: QSSA works better at $s \to 1$ (i.e., at $g \to 1$ or $\omega_0 \to 0$) while EA works better at $s \to 0$ (i.e., at $g \to 0$ or $\omega_0 \to 1$); the impact of $g$ is generally lesser than $\omega_0$. These results confirm those obtained in the previous study [6] for the five different scattering phase functions. An additional evaluation of methods' accuracy including consideration of intermediate $\omega_0$ values (0.3 and 0.7) was conducted using the direct numerical methods comparison (Fig. 5).

Calculations indicated that divergences between numerical methods are very small ($<1.8\%$) over the range of meaningful incoming angles with $\mu_1 > 0.66$, but may be relatively large at the small $\mu_1$. For example, at $\omega_0 < 0.8$ and $\mu_1 < 0.05$ divergences may reach 4–7% as shown in Fig. 5b, d, and f for the FFM phase function.

### 4.2. Development and verification of extended QSSA approximation

At $\mu_1 > 0.66$, errors of QSSA approximation are nearly independent relative to incoming geometry and flat in a function on $\omega_0$ (with minimum at $\omega_0 \to 0$ or $s \to 1$) (Fig. 4a and b). Accordingly, it is possible to extend QSSA toward greater values of

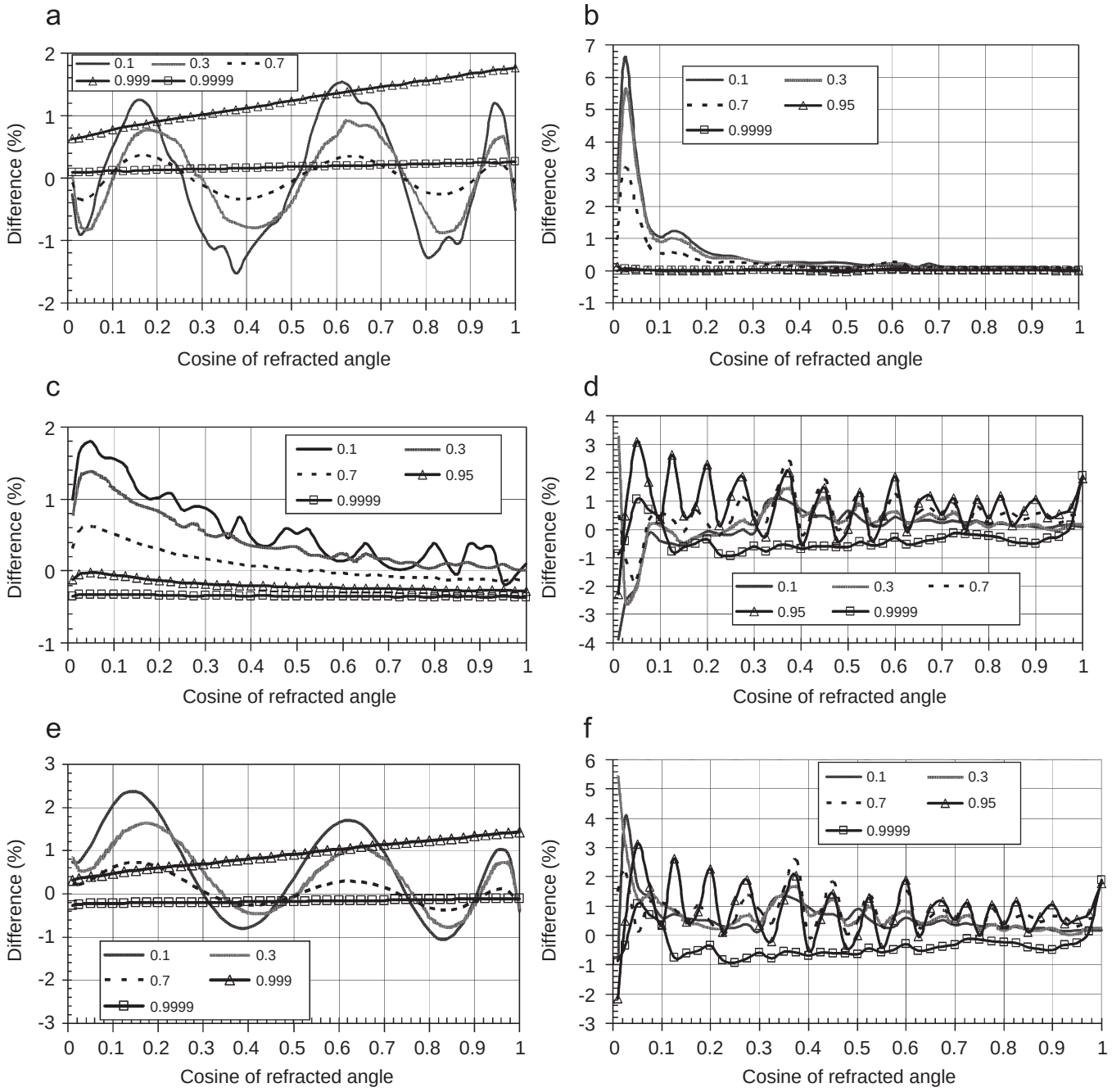


**Fig. 5.** Relative differences of plane albedo calculation between: DOM+MSH and IIM (a, b); RADUGA's and DOM+MSH (c, d) and RADUGA's and IIM (e, f) methods for the Rayleigh (a, c, e) and FFM (b, d, f) scattering phase functions.

$\omega_0$ comparing with an original approximation (Eq. (43)). The following simple quadratic approximation has been derived by polynomial least-squares fitting within the ranges of $\mu_1 \in [0.65; 1]$ and $\omega_0 \in [0.1; 0.9]$:

$$\Re(g, \omega_0, F, a_i, \mu_1) = \Re_{QSSA}(\omega_0, F, a_i, \mu_1)[1 + b_1(1-s) + b_2(1-s)^2], \tag{48}$$

where $\Re_{QSSA}$ is an original QSSA approximation; $b_1$, $b_2 = (-0.1534, 1.289)$ or $b_1$, $b_2 = (1.493, -1.361)$ for Rayleigh and FFM phase functions, respectively. The plots of errors for approximation (48) demonstrate (Fig. 6a and b) the significant improvement of the new "extended QSSA approximation" in comparison with initial QSSA approximation (Fig. 4a and b) for both the scattering phase functions.

The accuracy of the new approximation can also be compared with that of the extended Hapke approximation derived previously [7, Eqs. (35)–(37)] for the set of scattering phase functions with the asymmetry parameters $g \in [0.00; 0.96]$ in the form:

$$\Re(g, \omega_0, \mu_1) = \Phi(g, \omega_0, \mu_1)\frac{1-s}{1+2s\mu_1}, \tag{49}$$

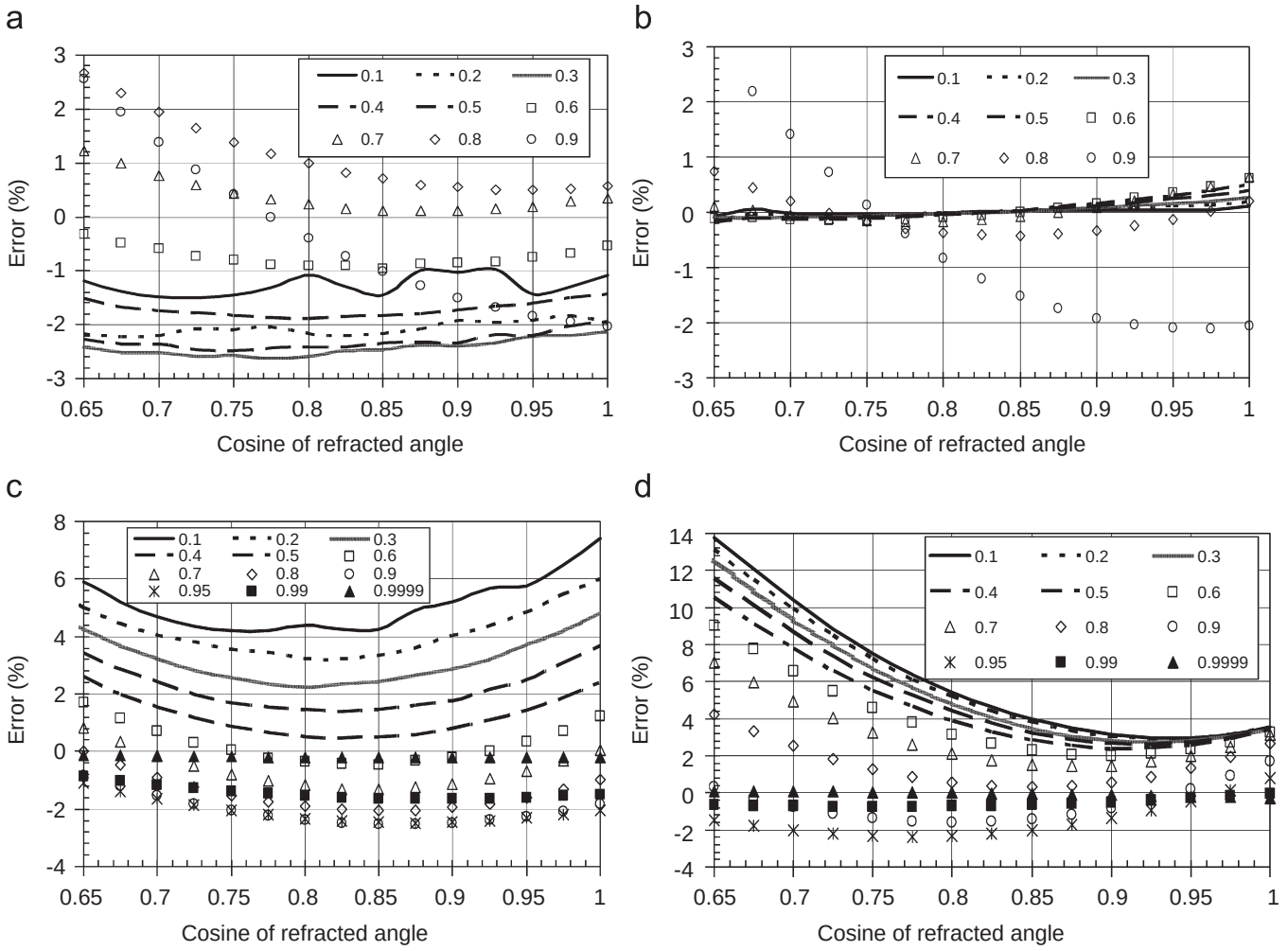


**Fig. 6.** Errors of extended QSSA approximation, Eq. (48) (a, b) and extended Hapke approximation, Eq. (49) (c, d) vs. DOM+MSH method for the Rayleigh (a, c) and FFM (b, d) scattering phase functions. Single-scattering albedo values shown in a legend.

where function $\Phi(g,\omega_0, \mu_1)$ is defined as

$$\Phi(g,\omega_0,\mu_1) = \exp\left\{\begin{array}{l}[(-0.991+3.139g-1.874g^2)\xi+(1.435-4.294g+2.089g^2)\xi^2]s \\ +[(0.719-5.801g+2.117g^2)\xi+(-0.509+0.418g+3.360g^2)\xi^2]s^2\end{array}\right\}, \quad (50)$$

where $\xi \equiv \mu_1 - 0.5$.

Fig. 6c and d represents the accuracy of approximation (49) versus DOM+MSH method for the Raleigh (Fig. 6c) and FFM (Fig. 6d) phase functions, respectively. Comparing Fig. 6c and d with Fig. 6(a and b) shows that for low values of $\omega_0$ (up to $\omega_0 \leqslant 0.8$), the extended QSSA approximation yields more accurate values of plane albedo, while for higher values $\omega_0$ results obtained by extended Hapke approximation are preferable. Combined plots for the plane albedo (for the both scattering phase functions) computed by extended QSSA (up to $\omega_0 \leqslant 0.8$) and extended Hapke (for $\omega_0 > 0.8$) approximations represented in Fig. 3 along with the results computed by numerical methods (IIM and DOM+MSH).

### 4.3. Particulate scattering phase function impact

All calculations of plane albedo by numerical methods shown above were performed assuming the Rayleigh or FFM scattering phase functions. It is clear that real $p(\chi)$ describing scattering by particles may substantially differ from the $p_{FFM}(\chi)$. This may lead to serious errors of calculations based on the $p_{FFM}(\chi)$ assumption. To show an impact of selected scattering phase functions on calculations of plane albedo, two other $p(\chi)$ typical for natural waters [6] were applied: one characterized very clear waters (with $g = 0.6962$, $F = 0.9411$) and the second very turbid waters (with $g = 0.9583$, $F = 0.9913$) (Fig. 7). All computations were performed for the same sets of $\omega_0$ (0.03, 0.05, 0.1, 0.2,…, 0.9, 0.99, 0.999, 0.9999) and $\theta_0$ (0°, 29.3°, 58.9°) by IIM method. As predicted, $\Re$ increases with increasing $\omega_0$ and $\theta_0$ and decreases with $F$.

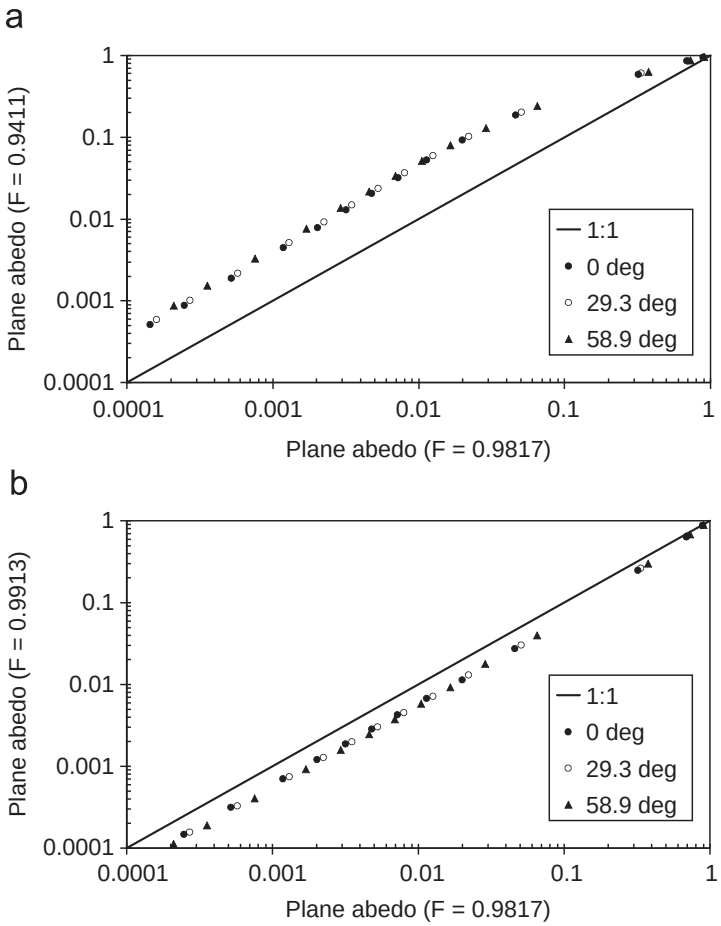


**Fig. 7.** Comparison of $\Re$ computed for the scattering phase function $p_{\mathrm{FFM}}(\chi)$ (with $g=0.9377$, $F=0.9817$) with (a) $\Re$ computed for very clear waters scattering phase function (with $g=0.6962$ and $F=0.9411$) and (b) $\Re$ computed for very turbid waters scattering phase function (with $g=0.9583$ and $F=0.9913$). All computations were performed for the same sets of $\omega_0$ (0.03, 0.05, 0.1, 0.2,…, 0.9, 0.99, 0.999, 0.9999) and $\theta_0$ (0°, 29.3°, 58.9°) by IIM method.

Errors arising from the information gap on the scattering phase function should be taken into account for solution of both the direct (estimation of reflectance from observed IOPs and lighting geometry) and inverse (estimation of IOPs from observed reflectance) optical problems. Obviously, additional *a priory* information about angular scattering (phase function) of underwater light fields is needed for more accurate analysis. This information may be obtained either from direct measurements or from different optical and bio-optical models. Further decreasing of errors in calculation of reflectance may be achieved also by the use of spectral reflectance ratios widely used in remote-sensing applications [45–48].

## 5. Conclusions

This study used three numerical methods to calculate plane albedo. They included: (1) IIM to iteratively solve the Ambartsumian's nonlinear integral equation; (2) DOM+MSH, which is a combination of discrete ordinate method for the regular part of RTE solution and a small angle modification of a spherical harmonics method for the singular anisotropic part of RTE solution; and (3) direct DOM (RADUGA code), which does not use any simplified assumptions. All three numerical methods yielded highly accurate plane albedo computational results for the molecular water (Rayleigh) and particulate matter (FFM) scattering phase functions $p(\chi)$, and for all ranges of optical parameters and lighting geometry common to natural waters. The high accuracy of these methods was confirmed by comparison with QSSA approximation at $\omega_0 \to 0$ (Fig. 4a and b) and with exponential approximation at $\omega_0 \to 1$ (Fig. 4c and d).

The differences between numerical methods using the Rayleigh $p(\chi)$ were $\leqslant 1.6\%$ for natural waters conditions and $\leqslant 2.4\%$ for the whole parameters ranges (Fig. 5e). For the $p_{FFM}(\chi)$, the maximum difference was 1.8% (Figs. 5d and f) and 6.6% (Fig. 5b) for the normal and the whole parameter ranges, respectively. We attributed these differences to the two reasons: (i) slightly different assignment of $p_{FFM}(\chi)$ for different numerical methods and (ii) the application of different assumptions and simplifications for different numerical methods.

Results indicated that the DOM+MSH method was preferable based on its accuracy and computer resource requirements. An additional advantage of this method was the capability to calculate different kinds of reflectance (both directional and

diffuse) within the layer. Both the DOM+MSH and RADUGA's methods provide modeled kinds of reflectance for any optical thickness. Additionally, a RADUGA's method may be especially appropriate for the solution of RTE in conditions of optically inhomogeneous media and for 2- and 3-D regions [25,43]. However, a reliable comparison of this direct method with the IIM and DOM+MSH methods for the FFM phase function was not possible because the phase function determination was slightly distinct for different methods. The results of the IIM method had similar high accuracies as the DOM+MSH and RADUGA's methods, but this method can only be used for semi-infinite or infinite turbid layers.

A new analytical method to extend QSSA approximation was developed for use in conjunction with early developed extended Hapke approximation, reducing errors to 2.7% (Fig. 6a and c) and 2.4% (Fig. 6b and d) for the Rayleigh and FFM $p(\chi)$, respectively. Thus, the accuracy of the combined (i.e., extended QSSA and extended Hapke) approximation is comparable to that of the numerical methods. The extended QSSA approximation was more suitable for both the phase functions considered at low values of $\omega_0$ (up to $\omega_0 \leqslant 0.8$). When $\omega_0 > 0.8$, the extended Hapke approximation would be preferable. In either case, we would expect an accuracy of separate approximations better than 14% (Fig. 6) for both phase functions, that is better than experimental precision achieved currently for reflectances [49,50].

Our calculation methods of the plane albedo should be applied in the context of the specific situation. This research compared numerical and analytical solutions for the plane albedo, but does not provide exact values of the plane albedo for any situation, caused, for example, by variable forms and sizes of water particles, and, hence, by different scattering phase functions. Computations performed for different phase functions demonstrated strong dependence of plane albedo on selected phase function. Because information about phase functions is not generally known for the typical underwater observations, the accurate computation of reflectance from IOPs and lighting geometry is still problematic. A solution of inverse task (estimation of IOPs from observed reflectance at known lighting geometry) would also be difficult, especially to find several IOPs simultaneously. Using spectral reflectance ratios and different approximations may favor the solution. For example, an extended Hapke approximation to plane albedo may be best applied to calculate direct and inverse underwater optical problems, since it incorporates only a small number of parameters and provides good accuracy across the entire range of natural waters parameters. However, additional research is required to further substantiate this conclusion.

## Acknowledgments

The authors would like to acknowledge Vladimir Haltrin, John Streicher and Peter Principle for their manuscript review comments and suggestions. Also, thanks are extended to M.I. Mishchenko for providing the IIM code used in support of this research. The United States Environmental Protection Agency (USEPA) funded and partially conducted the research described in this paper. Although this work was reviewed by EPA and has been approved for publication, it may not necessarily reflect official Agency policy. Mention of any trade names or commercial products does not constitute endorsement or recommendation for use. The USEPA provided funding to the National Research Council in support of this effort under Cooperative Agreement #CR-833232. Partial research funding was provided by the USEPA Global Earth Observation System of Systems (GEOSS) Advanced Monitoring Initiative (AMI) Grant #14.

## References

[1] Walker RE. Marine light field statistics. New York: Wiley; 1994.
[2] Preisendorfer RW. Hydrologic optics. Washington, DC: US Department of Commerce; 1976.
[3] Shifrin KS. Physical optics of ocean water. AIP translation series. New York: American Institute of Physics; 1988.
[4] Mobley CD. Light and water: radiative transfer in natural waters. San Diego, CA: Academic Press; 1994.
[5] Thomas GE, Stamnes K. Radiative transfer in the atmosphere and ocean. New York: Cambridge University Press; 2002.
[6] Kokhanovsky AA, Sokoletsky LG. Reflection of light from semi-infinite absorbing turbid media. Part 1: spherical albedo. Color Res Appl 2006;31:491–7.
[7] Kokhanovsky AA, Sokoletsky LG. Reflection of light from semi-infinite absorbing turbid media. Part 2: plane albedo and reflection function. Color Res Appl 2006;31:498–509.
[8] Mobley CD, Gentili B, Gordon HR, Jin Z, Kattawar GW, Morel A, et al. Comparison of numerical models for computing underwater light fields. Appl Opt 1993;32:7484–504.
[9] Kokhanovsky A. Optics of light scattering media. Chichester: Wiley; 2001.
[10] Ambartsumian VA. On the problem of the diffuse reflection of light. J Phys Acad Sci USSSR 1943;8:65–76.
[11] Budak VP, Korkin SV. The spatial polarization distribution over the dome of the sky for abnormal irradiance of the atmosphere. JQSRT 2008;109:1347–62.
[12] Chandrasekhar S. Radiative transfer. London: Oxford University Press; 1950.
[13] Zhang H, Voss KJ. Comparisons of bidirectional reflectance distribution function measurements on prepared particulate surfaces and radiative-transfer models. Appl Opt 2005;44:597–610.
[14] Mobley CD, Sundman LK, Boss E. Phase function effects on oceanic light fields. Appl Opt 2002;41:1035–50.
[15] Mishchenko MI, Dlugach JM, Yanovitskij EG, Zakharova NT. Bidirectional reflectance of flat, optically thick particulate layers: an efficient radiative transfer solution and applications to snow and soil surfaces. JQSRT 1999;63:409–32 [The FORTRAN code for calculation reflection function may be used freely from 〈http://www.giss.nasa.gov/~crmim/brf/〉].
[16] Stamnes K, Tsay SC, Wiscombe W, Jayaweera K. Numerically stable algorithm for discrete-ordinate-method radiative transfer in multiple scattering and emitting layered media. Appl Opt 1988;27:2502–9.
[17] Haltrin VI. Apparent optical properties of the sea illuminated by Sun and sky: case of the optically deep sea. Appl Opt 1998;37:8336–40.
[18] Sokoletsky L. Comparative analysis of selected radiative transfer approaches for aquatic environments. Appl Opt 2005;44:136–48.
[19] Hapke B. Theory of reflectance and emittance spectroscopy. New York: Cambridge University Press; 1993.

[20] Zibordi G. Marine optics: field radiometry. PhD dissertation, University of Southampton, UK, 2007.
[21] Gordon HR, Brown OB, Jacobs MM. Computed relationships between the inherent and apparent optical properties of a flat homogeneous ocean. Appl Opt 1975;14:417–27.
[22] Zhang H, Voss KJ. Bi-directional reflectance measurements of closely packed natural and prepared particulate surfaces. In: Kokhanovsky AA, editor. Light scattering reviews, vol. 3. Berlin: Springer; 2008. p. 279–328.
[23] van de Hulst HC. Multiple light scattering, vols. 1 and 2. New York: Academic; 1980.
[24] Haltrin VI, Gallegos SC. About nonlinear dependence of remote sensing and diffuse reflection coefficients on Gordon's parameter. In: Proceedings of the II international conference on current problems in optics of natural waters. ONW'2003, St. Petersburg, Russia, 2003. p. 363–9.
[25] Sokoletsky L. A comparative analysis of simple transfer approaches for aquatic environments. In: Proceedings of the 2004 ENVISAT and ERS symposium, Salzburg, Austria, 2004. ESA SP-572, CD-ROM.
[26] Nikolaeva OV, Bass LP, Germogenova TA, Kokhanovsky AA, Kuznetsov TS, Mayer B. The influence of neighboring clouds on the clear sky reflectance studied with the 3-D transport code RADUGA. JQSRT 2005;94:405–24.
[27] Nicodemus FE, Richmond JC, Hsia JJ, Ginsberg IW, Limperis T. Geometrical considerations and nomenclature for reflectance. National Bureau of Standards, US Department of Commerce, Washington, DC, 1977 〈http://physics.nist.gov/Divisions/Div844/facilities/specphoto/pdf/geoConsid.pdf〉.
[28] Gordon HG. Simple calculation of the diffuse reflectance of ocean. Appl Opt 1973;12:2803–4.
[29] Sathyendranath S, Platt T. The spectral irradiance field at the surface and in the interior of the ocean: a model for applications in oceanography and remote sensing. J Geophys Res 1988;93:9270–80.
[30] Haltrin VI. Theoretical and empirical phase functions for Monte Carlo calculations of light scattering in seawater. In: Proceedings of fourth international conference on remote sensing for marine and coastal environments. USA: Environmental Research Institute of Michigan; 1997. p. 509–18.
[31] Tzortziou M, Herman JR, Gallegos CL, Neale PJ, Subramaniam A, Harding Jr. LW, et al. Bio-optics of the Chesapeake Bay from measurements and radiative transfer closure. Estuarine Coastal Shelf Sci 2006;68:348–62.
[32] Weisstein EW. Fourier–Legendre series 〈http://mathworld.wolfram.com/Fourier-LegendreSeries.html〉.
[33] Weisstein EW. Legendre polynomial 〈http://mathworld.wolfram.com/LegendrePolynomial.html〉.
[34] Stokes G. On the intensity of light reflected from or transmitted through a pile of plates. Philos Mag 1862;24:480–9; Proc R Soc London 1862;11:545–56. Republished by the University of Michigan Library, 2005 〈http://quod.lib.umich.edu/cgi/t/text/text-idx?c=umhistmath;id-no=AAT0146.0004.001;cc=umhistmath〉.
[35] Tuckerman LB. On the intensity of the light reflected from or transmitted through a pile of plates. J Opt Soc Am 1947;37:818–9.
[36] Bellman RE, Wing GM. An introduction to invariant imbedding. New York: Wiley; 1975.
[37] Shifrin KS. Some remarks on the history of hydrological optics. In: Proceedings of the international conference on current problems in optics of natural waters (ONW'2001), St. Petersburg, Russia, 2001. p. 11–5.
[38] Goudsmit S, Saunderson JL. Multiple scattering of electrons. Phys Rev 1940;58:24–9;
Goudsmit S, Saunderson JL. Multiply scattering of electrons. II. Phys Rev 1940;58:36–42.
[39] Karp AH, Greenstadt J, Fillmore JA. Radiative transfer through an arbitrary thick scattering atmosphere. JQSRT 1980;24:391–406.
[40] Budak VP, Korkin SV. On the solution of a vectorial radiative transfer equation in an arbitrary three-dimension turbid medium with anisotropic scattering. JQSRT 2007; doi:10.1016/j.jqsrt.2007.08.016.
[41] Davidson B. Neutron transport theory. Oxford: Oxford University Press; 1957.
[42] Joint Supercomputer Center. High-end computing. MVS-15000BM 〈http://www.jscc.ru/cgi-bin/show.cgi?path=/hard/mvs15000bm.html&type=3〉.
[43] Nikolaeva OV, Bass LP, Germogenova TA, Kuznetsov VS. Algorithms to calculation of radiative fields from localized sources via the Code Raduga-5.1(P). Transp Theory Stat Phys 2007;36:439–74.
[44] Anikonov AS, Ermolaev SY. On diffuse light reflection from a semiinfinite atmosphere with a highly extended phase function. Vestnik LGU 1977;7:131–7.
[45] O'Reilly JE, Maritorena S, Mitchell BG, Siegel DA, Carder KL, Garver SA, et al. Ocean color chlorophyll algorithms for SeaWiFS. J Geophys Res 1998;103:24937–53.
[46] Ruddick KG, Gons HJ, Rijkeboer M, Tistone G. Optical remote sensing of chlorophyll *a* in case 2 waters by use of an adaptive two-band algorithm with optimal error properties. Appl Opt 2001;40:3575–85.
[47] Doxaran D, Cherukuru RC, Lavender SJ. Use of reflectance ratios to estimate suspended and dissolved matter concentrations in estuarine waters. Int J Remote Sensing 2005;26:1763–9.
[48] Gitelson AA, Schalles JF, Hladik CM. Remote chlorophyll-*a* retrieval in turbid, productive estuaries: Chesapeake Bay case study. Remote Sensing Environ 2007;109:464–72.
[49] Toole DA, Siegel DA, Menzies DW, Neumann MJ, Smith RC. Remote-sensing reflectance determinations in the coastal ocean environment: impact of instrumental characteristics and environmental variability. Appl Opt 2000;39:456–69.
[50] Ouillon S, Petrenko AA. Above-water measurements of reflectance and chlorophyll-a algorithms in the Gulf of Lions, NW Mediterranean Sea. Optics Express 2005;13:2531–48.